INSTITUTE OF PHYSICS PUBLISHING JOURNAL OF PHYSICS B: ATOMIC, MOLECULAR AND OPTICAL PHYSICS

J. Phys. B: At. Mol. Opt. Phys. **38** (2005) 975–1000 doi:10.1088/0953-4075/38/7/016

Comparison of hydrogen Balmer-alpha Stark profiles measured at high electron densities with theoretical results

Hans R Griem[1], **Jacek Halenka**[2] **and Wieslaw Olchawa**[2]

[1] Institute for Research in Electronics and Applied Physics, University of Maryland, College Park, MD 20742, USA
[2] Opole University, Institute of Physics, Oleska 4845-052 Opole, Poland

E-mail: griem@umd.edu

Received 3 September 2004
Published 22 March 2005
Online at stacks.iop.org/JPhysB/38/975

Abstract

Profiles of the H-alpha line calculated using the full computer simulation method (FCSM) and the standard theory (ST) agree excellently with a measured profile (at an electron density of $N_e = 9.0 \times 10^{16}\,\mathrm{cm}^{-3}$ and temperature $T = 12\,600$ K) in an argon–hydrogen (minority) arc plasma. Calculated widths (FCSM) and shifts (ST) also agree well with experimental data from flash-tube plasmas and gas-linear pinch plasmas. Some discrepancies are probably caused by experimental flaws. Our analysis of the so-called generalized theory (GT) shows that this theory is burdened with un-physical approximations, and consequently so are all subsequent modifications based on GT. It is shown that the so-called acceleration of the electron by the ion field (AEIF) effect is no new effect, but only a drastically simplified alternative model involving physical and algebraic errors, compared with traditional theory (ST, FCSM, etc) of the ion–electron interactions. A corrected, but still somewhat faulty, AEIF model yields an up to 15% increase of the half width of the H-alpha line (about 10% being contributed by unavoidable approximations and 3–5% by the pure AEIF effect, and worsening the agreement with experimental data) in contrast to the originally reported 25% decrease of the half width. Finally, we find that for plasma parameters $\Gamma \leqslant 0.25$ there is neither theoretical nor experimental evidence for the existence of the new 'warm dense matter effects' claimed in Escarguel *et al* (2000 *Phys. Rev.* E **62** 2667), Flih *et al* (2003 *J. Phys. B: At. Mol. Opt. Phys.* **36** 283), Escarguel *et al* (2000 *J. Quant. Spectrosc. Radiat. Transfer* **64** 353) and Flih and Vitel (2001 *Proc. 15th Int. Conf. on Spectral Line Shapes*).

1. Introduction

Investigations of shapes and shifts of hydrogen lines emitted by plasmas are fundamental to atomic plasma spectroscopy. These studies are also important due to applications in plasma diagnostics and in astrophysics for the interpretation of the stellar spectra, especially of white dwarfs. The half widths of the hydrogen lines are a simple and good tool for the electron density determination. However, precise knowledge about the shifts of these lines allows an accurate reduction of the so-called observed residual (after subtraction of the Doppler effect due to the star's motion) red shifts by contributions caused by pressure effects. On the basis of these gravitational red shifts reduced in this way from the plasma effects it is possible to determine the ratio M/R, where M is the mass and R the radius of the white dwarf. The importance of this effect was shown in papers [1, 2].

A review of the state of the theoretical and experimental studies of the spectral line shapes, with special consideration of the H_α line emitted by dense plasmas, was presented in [3, 4]. The aim of this paper is to assess the new theoretical and experimental results for the H_α line formed in dense plasmas, after the year 2000.

Such new theoretical results were reported in [5–13], whereas the new experimental data are published in [12–17]. In [5–8] H_α line profiles have been calculated within the so-called full computer simulation method (FCSM), i.e. the total electric field, produced by ions and electrons, has been simulated, whereas the corresponding Schrödinger equation was solved numerically. In [5] the full width at half maximum (FWHM) was calculated for the first few lines of the Lyman and Balmer series in a helium plasma, assuming a small amount of hydrogen. It was found that the ratio of H_α FWHM in plasmas, with only He^{++} ions to FWHM values in plasmas with only He^{+} ions, is very close to 1. This result is important for the interpretation of H_α line shapes measured in the so-called Bochum experiments [17, 18]. In [6] asymmetric and shifted profiles of the H_α line were calculated within the FCSM for the first time. In these simulations the inhomogeneity of the microfields produced by ions and by electrons was taken into account. Calculations were performed up to second order in the perturbation theory (the quadratic Stark effect for the microfield varying in time). It was found, that within this approximation [6], the value of FWHM is almost independent of the minimal emitter–perturber distance; however, the value of the red shift is sensitive to this parameter. In [7] the values of FWHM were calculated for the first few lines of the Balmer series for non-LTE plasmas. In the case of dense plasmas, being the subject of interest in this paper, this result is not essential, because in these dense plasmas ($N_e > 10^{17}\,cm^{-3}$) LTE conditions are very well satisfied. In the approximation [8] fine structure and Stark–Doppler coupling are taken into account. This is important only in the case of low N_e.

In [12, 13], on the basis of earlier publications [9–11, 19, 20] the theory, which the authors of [13] have called the Oks' theory, was executed. This theory is quasistatic for ion effects, completed by corrections for ion dynamical effects. The authors of [12, 13] reported that Oks' advanced generalized theory (AGT) gives values of FWHM and red shifts for the H_α line agreeing very well with experimental data for strongly coupled plasmas [12–14], i.e. for plasmas having high electron density, $N_e \sim 10^{18}\,cm^{-3}$, and moderate temperature $T \sim 10^4\,K$. The authors claim that their measurements confirm and explain 'new warm dense matter' effects predicted by this theory. Simultaneously, the authors of [12, 13] emphasize very large discrepancies of the experimental results [12–14] with the so-called standard quasistatic theory (ST) [21–25]. In paper [26] it was shown that this statement is not justified. In various comments [27–29] and in [30] problems with the AGT and critical remarks about the experiments [12–14] were presented. In papers [29, 30] it was shown that the model of a new source of shifts

of hydrogen spectral lines introduced in [20] actually gives values of the shifts exactly equal to zero.

Following the pioneering papers [31, 32], in which the computer simulation method was first used for hydrogen line profile calculations, this method has been developed and tested in a few research centres (independently from each other), see, e.g. [33–37], and is currently well recognized. FCSM results agree very well with measurements, with the exception of [12, 14] and the first Bochum experiment [18], for N_e close to 10^{19} cm^{-3}. The state of the AGT theory is the opposite; it requires independent (additional) tests. Therefore, in this paper we focused our attention first of all on this theory. In section 2 we carried out a review of this theory. In the AGT paper [10] a 'new warm dense matter effect' (the so-called 'acceleration of the perturbing electrons by the ion field' (AEIF)) was introduced into the Stark broadening profile theory. Our evaluation of the AEIF is presented in section 3. In order to verify our calculations, we have measured the H_α profile formed within an arc plasma. The wall-stabilized arc is a very well examined plasma source. It allows us to produce a homogeneous (along the arc axis), stationary and optically thin plasma layer. Such features allow optimal measurements of the line profile, in contrast to other plasma sources. Our experiment is described in section 4. Experiments [12, 14], in which the H_α profiles were formed in underwater laser sparks, were discussed in comments [27, 29]. In these comments, serious errors made in [12, 14] were pointed out, in particular in the self-absorption correction procedure for these inhomogeneous and optically thick plasma. As was shown in comment [29], if the plasma parameters reported in [12, 14] were correct, then such plasma would have 1.5 times higher density than the normal water density, or more. In section 5, where measurements are compared with theory, results [12, 14] are therefore omitted as nonrealistic. In section 6 we present our conclusions. In the appendix information is gathered about calculations of the probability distribution function for electric microfields in plasmas needed for the H_α line profile calculations under the physical conditions corresponding to the experiments discussed here.

2. Review of the advanced generalized theory

In paper [13] the numerical values of the half widths and shifts of the H_α line presented as results of the AGT theory were found to be in excellent agreement with the measurements reported in the same paper. This theory consists of four main parts:

(i) the so-called generalized theory GT [9, 19],
(ii) a model for the sources of the shifts of a spectral line [20],
(iii) a model describing mechanisms for the reductions of widths and shifts of a spectral line due to the acceleration of (perturbing) electrons by the ion field (AEIF) [10, 11],
(iv) a model for the contribution of ion dynamics to the line broadening [13].

Below we present problems with this theory and the various models.

Firstly, the standard theory (ST) of hydrogen line profiles [21, 22], as well as GT, were formulated within the quasistatic approximation for ions and the impact, binary approximation for electrons. The starting point of both theories is the Hamiltonian

$$H = H_0 - \mathbf{d} \cdot \mathbf{F}, \tag{1}$$

where H_0 is the Hamiltonian of an isolated hydrogen atom, $\mathbf{d}$ is the electric dipole moment of the atom, whereas $\mathbf{F}$ is the resultant electric microfield in the plasma produced by ions and electrons. The product $\mathbf{d} \cdot \mathbf{F}$, representing the plasma–emitter interaction, is the first term in the multipole expansion, which is appropriate only when the following inequality is satisfied:

$$|\mathbf{r}| < |\mathbf{R}_k|, \tag{2}$$

where $\mathbf{r}$ represents the location of the bound electron, and $\mathbf{R}_k$ is the location of a perturber, both relative to the atomic nucleus. Within ST the independence of the electronic and ionic microfields is assumed, whereas in GT the coupling of the electronic and ionic field is taken into consideration, in consequence of which the impact operator Φ_{if} in GT depends also on the ion field. (Note that this *coupling* is always included in FCSM.) Such generalization of GT causes the matrix elements of the Φ_{if} operator not to be divergent formally for the shifted Stark components, even when the impact parameter ρ reaches zero. (Within ST and for the unshifted components in AGT—in order to avoid such divergence—a minimum value $\rho_{\min}$ is introduced and contributions of strong collisions are evaluated approximately.) However, this generalization of GT is dubious, because (i) the calculations are carried out within the straight classical path approximation for electrons, i.e. allowing the free electrons to penetrate into the excited atomic interior, which becomes a serious problem; (ii) for values of ρ near zero the condition given by equation (2) is not satisfied, so this becomes inconsistent with the Hamiltonian equation (1). Consequently, for small values of ρ the GT theory gives erroneous results. All numerical values of the half widths of the hydrogen spectral lines gathered in [9] suffer from this defect.

Secondly, the basis of the model for the shift of hydrogen spectral lines in [20] are calculations in [38], where the Stark shifts (of the line components) are produced by collisions (within the binary impact approximation) of electrons with an emitter (within the pure dipole approximation). However, in the same paper [38] the authors report that these shifts become nearly equal to zero when the Debye screening effect is taken into account. In the new theory this fact, as was shown in [27, 28], is completely ignored. Even more, it is evident—from [30] analytically and from [29] numerically—that within the pure dipole approximation and assuming atomic and perturber density matrices to be independent of each other, these shifts are exactly equal to zero.

Thirdly, in [10], where the AEIF effect within GT was formulated for the first time, equations (3) and (4) contain essential errors (see also section 3). Additional errors cause GT to give unphysical results (cf the first point above). Therefore we have re-calculated (in section 3) the influence of the AEIF effect on hydrogen spectral line shapes within ST and, using a computer simulation method, simultaneously introduced improvements of the AEIF effect model.

Fourthly, when two mechanisms of the spectral line broadening are statistically independent of each other, the resultant line profile can be calculated as a convolution of line profiles produced by each of these broadening mechanisms. In the AGT theory [13] this condition of statistical independence is ignored. The convolution is made of two line profiles: (i) a profile produced by electrons (within the binary impact approximation, including the AEIF effect), and by ions within the quasistatic approximation, P_1, and (ii) the line profile formed by the same ions, but within the dynamical adiabatic approximation, P_2. These two line profiles are not only formed by two statistically interdependent line broadening mechanisms, but this procedure also takes into account the broadening effects by the same ions twice, only with different approximations. Actually, the quasistatic line profile P_1 should be produced only by the quasistatic fraction of ions (which produce the electric field $\mathbf{F}_q$) and by electrons, and the profile P_2, only by the dynamical fraction of ions (which produce the electric field $\mathbf{F}_d(t)$). Therefore, in order to calculate P_1 other field strength distribution functions should be used than those known from the literature [39–41]. These functions from the literature $W_a(\beta)$ were calculated taking into account all ions. Moreover, obviously the adiabatic approximation (i.e. assuming $\mathbf{F}_d(t) \parallel \mathbf{F}_q$) for the P_2 profile calculation used in [13] in order to describe the ion dynamics is entirely inappropriate for the H_α line profile. In the case of this line the central Stark component is of crucial importance, but the contribution of the adiabatic fraction to the

ion-dynamical broadening of the unshifted line components (when $\mathbf{F}_d(t) \parallel \mathbf{F}_q$) is exactly equal to zero. The ion-dynamical broadening of the central component of the H_α line is actually caused by the nonparallel field components, i.e. $\mathbf{F}_d(t)$ nonparallel to $\mathbf{F}_q$. The ion-dynamical broadening used in AGT contributes only to the shifted Stark components.

In summary, the agreement between the AGT theory and the measurements reported in [13] and also with the unrealistic experimental data in [12, 14] must be regarded as being coincidental, as already emphasized in [26, 42].

3. Influence of ion–electron interactions on H_α line width

The Hamiltonian of a typical emitter in a plasma can be described as follows:

$$H = H_0 - U_{\mathrm{ai}} + U_{\mathrm{ae}} + U_{\mathrm{ie}}, \tag{3}$$

where H_0 is the Hamiltonian of the isolated emitter, U_{ai} represents the emitter–ion and ion–ion interaction, U_{ae} is the emitter–electron and electron–electron interaction, whereas U_{ie} is the operator of ion–electron interactions. The interactions between the neutrals, i.e. atoms, were neglected. Within the traditional theories of the spectral line profiles (e.g. ST, FCSM and others) in the next step, a simplification is introduced, owing to which the interaction U_{ie} can be taken into consideration. Namely, averaging over time (short in relation to the ionic relaxation time, $\tau_{\mathrm{i}} \approx R_{\mathrm{i}}/\langle v_{\mathrm{i}}\rangle$, and, at the same time, long in relation to the electronic relaxation time, $\tau_{\mathrm{e}} \approx R_{\mathrm{e}}/\langle v_{\mathrm{e}}\rangle$, where R_{i} and R_{e} describe the mean ion and electron distances, respectively, whereas $\langle v_{\mathrm{i}}\rangle$ and $\langle v_{\mathrm{e}}\rangle$ are the mean ion and electron thermal velocities) one obtains the potential at the point $\mathbf{r}$ produced by the statistical kth ion at position $\mathbf{R}_k^{(\mathrm{i})}$ in the sea of the free electrons from the Poisson equation

$$\nabla^2\phi_k^{(\mathrm{i})}(\mathbf{r}) = -4\pi e N_{\mathrm{e}}\big(1 - \exp\big(-\mathrm{e}\,\phi_k^{(\mathrm{i})}(\mathbf{r})/kT\big)\big) - 4\pi Z_k e\delta\big(\mathbf{r} - \mathbf{R}_k^{(\mathrm{i})}\big). \tag{4}$$

If the plasma parameter Γ satisfies the relation, e.g. [23],

$$\Gamma = \big\langle e\phi_k^{(\mathrm{i})}(\mathbf{r})\big\rangle\big/kT = \tfrac{1}{3}Z_k^{5/3}a^2 \ll 1, \tag{5}$$

where k is the Boltzmann constant, T is the temperature, $Z_k e$ is the electric charge of the perturbing ion, $a = R_0/D$ is the screening parameter with $D = \sqrt{kT/(4\pi e^2 N_{\mathrm{e}})}$ the Debye length and R_0 the distance defined by the relationship $(4/15)(2\pi)^{3/2}R_0^3 N_{\mathrm{e}} = 1$ (see, e.g. [39]), we obtain the Debye potential

$$\phi_k^{(\mathrm{i})}(\mathbf{r}) = \frac{Z_k e}{\big|\mathbf{r} - \mathbf{R}_k^{(\mathrm{i})}\big|}\exp\big(-\big|\mathbf{r} - \mathbf{R}_k^{(\mathrm{i})}\big|\big/D\big). \tag{6}$$

The resulting strength of the electric microfield at an arbitrary point of the coordinate $\mathbf{r}$ is

$$\mathbf{F}^{(\mathrm{i})}(\mathbf{r}) = -\nabla\left(\sum_{k=1}^{N}\phi_k^{(\mathrm{i})}(\mathbf{r})\right) = \sum_{k=1}^{N} Z_k e\left(1 + \frac{\big|\mathbf{r} - \mathbf{R}_k^{(\mathrm{i})}\big|}{D}\right)\exp\big(-\big|\mathbf{r} - \mathbf{R}_k^{(\mathrm{i})}\big|\big/D\big)\frac{\big(\mathbf{r} - \mathbf{R}_k^{(\mathrm{i})}\big)}{\big|\mathbf{r} - \mathbf{R}_k^{(\mathrm{i})}\big|^3}. \tag{7}$$

It is produced by *pseudo-ions*, and is usually called the low-frequency field component, contrary to the high-frequency component produced by electrons. In the case of strongly coupled plasmas, i.e. when the plasma parameter does not fulfil the relation given by equation (5), the potential $\phi^{(\mathrm{i})}$ resulting from equation (4), is an even shorter-range potential than the Debye potential. For all experiments mentioned in the introduction, the plasma parameters satisfy the relation $\Gamma < 0.25$; therefore the above model of interactions is valid for the purposes of this paper. In this way the real plasma is replaced by an artificial system consisting of the emitter, electrons and *pseudo-ions*, within which electrons and *pseudo-ions* do

not interact mutually. The interactions between the *pseudo-ions* are taken into account within the procedure of the probability distribution function $W_a(\beta)$ calculation, where $F^{(\mathrm{i})} = |\mathbf{F}^{(\mathrm{i})}(0)|$ is expressed in the reduced scale $\beta = F^{(\mathrm{i})}/F_0$, and the Holtsmark field strength is equal to $F_0 = e\big/R_0^2$. The distribution functions of these field-strengths given by equation (7) in the case of plasmas consisting of singly charged ions only, $Z_k = 1$, were calculated in [39–41]. As was shown, e.g. in [37], the electron–electron interactions are reproduced satisfactorily, when the real electrons are replaced by *pseudo-electrons* with Coulomb potentials cut-off at the Debye length D (i.e. the effect of collisions with electrons of impact parameters greater than D is reduced to zero):

$$\mathbf{F}^{(\mathrm{e})}(0) = \begin{cases} \sum_{k=1}^{N} e\mathbf{R}_k^{(\mathrm{e})}\big/\big|\mathbf{R}_k^{(\mathrm{e})}\big|^3 & \text{for} \quad \rho \leqslant D, \\ 0 & \text{for} \quad \rho > D, \end{cases} \tag{8}$$

similar to the ST theory. Finally, one obtains a system consisting of free *pseudo-electrons* and *pseudo-ions* interacting with the emitter. Within this model, commonly used in theories of spectral line profiles in plasmas, the straight-line, constant velocity trajectory of the perturbing electrons is completely justified. So, the Hamiltonian given by equation (3) can be written as follows:

$$H = H_0 - \mathbf{d} \cdot [\mathbf{F}^{(\mathrm{i})}(0) + \mathbf{F}^{(\mathrm{e})}(0)] + \cdots, \tag{9}$$

where $\mathbf{F}^{(\mathrm{i})}(0)$ and $\mathbf{F}^{(\mathrm{e})}(0)$ are the resulting field-strengths given by equations (7) and (8), respectively, at the point where the emitter is located. When the interaction U_{ie} in the Hamiltonian equation (3) is neglected, the potential of the perturbing ions remains the Coulomb potential. Consequently, the Hamiltonian given by equation (3) becomes

$$H = H_0 - \mathbf{d} \cdot \big[\mathbf{F}_c^{(\mathrm{i})}(0) + \mathbf{F}^{(\mathrm{e})}(0)\big] + \cdots, \tag{10}$$

where the resulting microfield, produced by ions, is described as follows:

$$\mathbf{F}_c^{(\mathrm{i})}(0) = -\sum_{k=1}^{N} Z_k e\big(\mathbf{R}_k^{(\mathrm{i})}\big)\big/\big|\mathbf{R}_k^{(\mathrm{i})}\big|^3. \tag{11}$$

This means that the probability distribution function $W_a^{(c)}(\beta)$ for the Coulomb plasma microfields is numerically equal to the high-frequency component $W_a^{(h)}(\beta)$ calculated by Hooper in [43]. In figure 1 we compare the distribution functions $W_a(\beta)$ of the microfield given by equation (7) (at $\mathbf{r} = \mathbf{0}$), and $W_a^{(c)}(\beta)$ of the microfield given by equation (11), for the screening parameter 0.9, which approximately corresponds to the experiments in [12–14]. (For the calculations of these functions see the appendix.) In figure 1 we see that the function $W_a^{(c)}(\beta)$ predicts higher values of the field-strengths than the $W_a(\beta)$ function. Consequently, the FWHM_c values, calculated using the Hamiltonian given by equation (10) and the $W_a^{(c)}(\beta)$ function, will be greater than those calculated using the traditional Hamiltonian equation (9) and the $W_a(\beta)$ functions. In figure 2 we present the relative differences of the $\mathrm{FWHM}_{\mathrm{ie}}$ values for H_α when the U_{ie} term in the Hamiltonian is (or is not) omitted. (The values of N_{e} indicated in figure 2 were related to the values of T as follows: for $N_{\mathrm{e}} \leqslant 10^{17}\,\mathrm{cm}^{-3}$ we took temperatures appropriate for the arc plasmas, and, for $N_{\mathrm{e}} > 10^{17}\,\mathrm{cm}^{-3}$, those appropriate for flash-tube plasmas.) The calculations have been performed within the dipole approximation and using the FCSM method, similarly as in the earlier work [44]. We see, in particular, that the ion–electron interactions lead to a narrowing of the spectral line profile relative to the line-shape, for which these interactions are neglected. Of course, in all traditional (e.g. ST, MMM, FCSM, etc) line shape theories, these ion–electron interactions are taken into account.

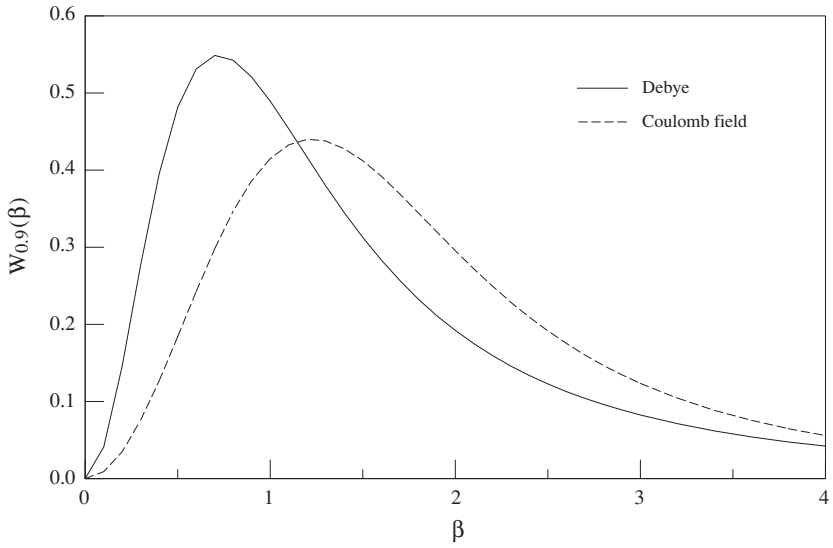

Figure 1. Comparison of the electric microfield distributions function $W_{0.9}(\beta)$ (for the Debye field) and $W_{0.9}^{(c)}(\beta)$ (for the Coulomb field) at a neutral point as a function of the reduced electric field strength β for perturbing ions of charge 1 and for the screening parameter $a = 0.9$.

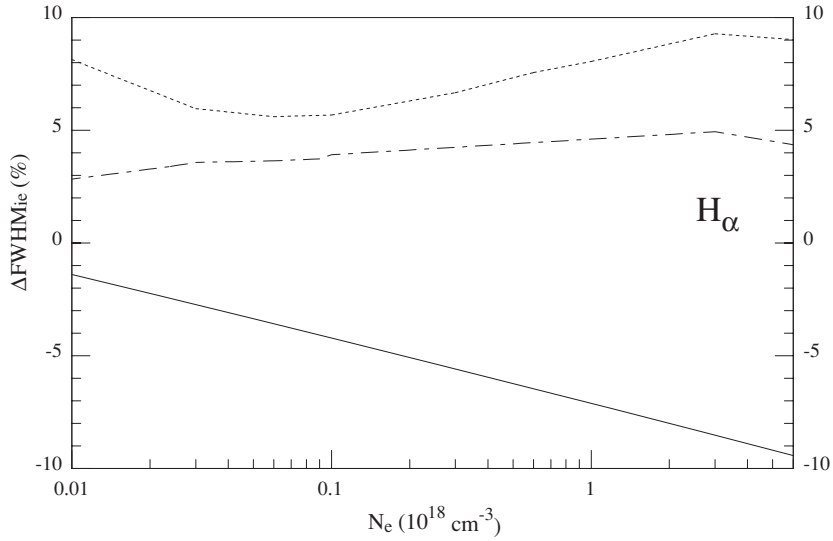

Figure 2. The relative change of H-alpha line width $\Delta\text{FWHM}_{\text{ie}} = 100\%$ (FWHM − FWHM_{c})/FWHM versus electron density. Values of FWHM were obtained for the full Hamiltonian given by equation (3), whereas values of FWHM_{c} with the last term U_{ie} (ion–electron interactions) omitted in this Hamiltonian. The line —— concerns calculations within an FCSM approximation similar to [44]. The other lines represent, corrected in this paper, results within the alternative model for ion–electron interactions, the so-called AEIF model. The line — · — corresponds to the AEIF contribution when the dynamic effect is included. The line · · · · · · shows the complete AEIF effect in the quasistatic approximation.

In [10], an alternative model of the ion–electron interactions, U_{ie}, compared with the one just described, is proposed. Namely, the author of [10] proposes a drastically simplified model,

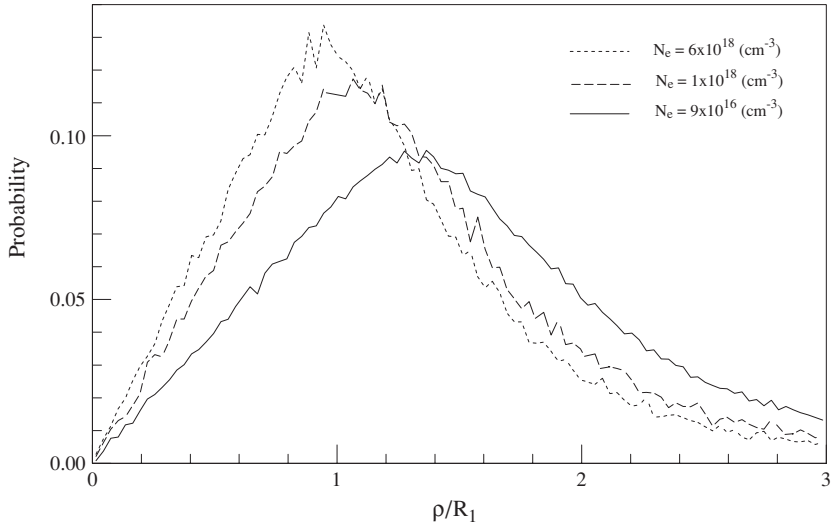

Figure 3. Probability density of ρ/R_1. ρ is the emitter–electron impact parameter and R_1 is the emitter–nearest perturbing ion distance.

within which only the velocity change of the nearest (with respect to the emitter) electron, in the field of the single, nearest ion, is taken into account, with the following additional restriction (third line of section 2 in [10]):

$$\rho \ll R_1, \tag{12}$$

where ρ is the emitter–electron impact parameter and R_1 is the emitter–nearest perturbing ion distance. This condition was accepted in [10] in order to justify the assumption that the emitter–electron and the emitter–ion distances are approximately equal. As shown in figure 3, the condition given by equation (12) is not satisfied in most of the cases. The functions presented in figure 3 have been calculated using the computer simulation method for electron densities indicated in the figure and temperatures 20 000 K, 13 000 K and 12 600 K, respectively. The first two temperatures correspond to the flash-tube plasma [13], the last temperature corresponds to the arc plasma described in section 4 of this paper.

The basic idea in [10], under condition (12), is allowing in the impact operator Φ_{if} (within the ST approximation) for the changing electron velocity V due to the interaction with the nearest ion of the charge number Z at distance R_1 from the emitter. Then, the velocity V results from the energy balance

$$\tfrac{1}{2}mV^2 \approx \tfrac{1}{2}mv^2 + Ze^2/R_1. \tag{13}$$

The next equations in [10] have the following form:

(i) dependence of the impact operator $\Phi_{if}^{\mathrm{ST}}(v)$ on the thermal velocity of the perturbing electron

$$\Phi_{if}^{\mathrm{ST}}(v) = K_{if}/v^2, \tag{14}$$

where

$$K_{if} = -\frac{4\pi}{3}\frac{e^4}{\hbar^2}N_{\mathrm{e}}(\mathbf{r}_i \cdot \mathbf{r}_i - 2\mathbf{r}_i \cdot \mathbf{r}_f^* + \mathbf{r}_f^* \cdot \mathbf{r}_f^*)\left(\ln\frac{\rho_{\max}(v)}{\rho_{\min}(v)} + \frac{1}{2}\right), \tag{15}$$

and the limiting electron impact parameters are

$$\rho_{\max} = \min(v/\omega, D), \tag{16}$$

and

$$\rho_{\min} = \frac{\hbar}{mv}\left(n_i^2 - n_f^2\right); \tag{17}$$

(ii) the expression introducing the AEIF effect into the impact operator was

$$\Phi_{if}^{\mathrm{AEIF}}(v) = \Phi_{if}^{\mathrm{ST}}(V). \tag{18}$$

After averaging over the Maxwell distribution $M(v) = 4\pi^{-1/2}v_T^{-3}v^2\exp\left(-v^2/v_T^2\right)$ (where $v_T = (2kT/m)^{1/2}$) this becomes

$$\Phi_{if}^{\mathrm{AEIF}}(R_1) = f(R_1, T)\Phi_{if}^{\mathrm{ST}}. \tag{19}$$

We take note that the above formulae include the algebraic error in equation (14) (the velocity of the perturbing electron appears in the (-2) power instead of the (-1) power) and consequently an error in the function $f(R_1, T)$ and a model error from using equation (18). In the ST approximation (cf equation (3) of [21], equation (110) of [22], equation (5.14) of [55] or equation (7.3.32) of [56]), the dependence on the velocity of perturbing electron is as follows:

$$\Phi_{if}^{\mathrm{ST}}(v) = K_{if}/v. \tag{20}$$

In ST the impact operator Φ_{if}^{ST} is calculated under the assumption that the probability density of the thermal velocity $\mathbf{v}$ is isotropic with respect to the centre of symmetry coinciding with the centre of the emitter. As mentioned in the beginning of this section, the pseudo-electrons influence the field distributions, but do not interact with each other nor with the ions. Therefore, the operator Φ_{if}^{ST} has been calculated for the straight-line trajectory of the *pseudo-electrons* and for the isotropic (relative to the emitter) probability density of the electron velocity $\mathbf{v}$. Then, after averaging over angles, the following relations result from the symmetry (see page 75 in [53]):

$$\{v_x v_x\} = v^2/3, \qquad \{v_x v_y\} = 0, \qquad \{v_x \rho_x\} = \{v_x \rho_y\} = 0, \text{ etc.} \tag{21}$$

Due to the above relations only a few matrix elements of the Φ_{if}^{ST} operator are different from zero. In the AEIF model the electron–nearest ion interaction breaks the symmetry given by (21) and, therefore, many more non-zero matrix elements of $\Phi_{if}^{\mathrm{AEIF}}$ should appear than in ST.

Apart from the already mentioned defects of the AEIF, some more occur. The position of the nearest ion R_1 should be correlated with the value of the strength of the local ionic electric field β. As a consequence of the description of the U_{ie} interactions via the operator Φ_{if} in the AEIF model, Coulomb potentials were used for the description of the emitter–ion interactions U_{ai} and, consequently, the $W_a^{(c)}(\beta)$ probability distribution function should have been used. Both problems under consideration here were ignored in [10]. The construction of a correct model of the interaction U_{ie} via the operator Φ_{if}, i.e. departures from condition $\rho \ll R_1$ and, simultaneously, from (18) would have required time-consuming and difficult calculations. Therefore, we performed only estimates, which are free from the error in equation (14) and which take the dependence of R_1 on β and the distribution function $W_a^{(c)}(\beta)$ into account. Such a recalculated $f(R_1, T)$ function for equation (19) is

$$f_a(\beta) = \begin{cases} \frac{4}{\sqrt{x}}\int_0^\infty \left(1 + \frac{1}{3}a^2\beta^{1/2}x^{-2}\right)x^2\,\mathrm{e}^{-x^2}\,\mathrm{d}x & \text{for} \quad \beta \leqslant \beta_c, \\ 1 & \text{for} \quad \beta > \beta_c. \end{cases} \tag{22}$$

The correction term $\frac{1}{3}a^2\beta^{1/2}x^{-2}$ accounts for the increase of the electron velocity from the attraction by the nearest ion, see equation (13). We assume that β is connected with R_1 by $\beta = F_1/F_0 = (R_0/R_1)^2$, i.e. the total ionic field is produced by the nearest ion. (Of course, this is a simplification, because the exact relation between R_1 and β is determined by a joint

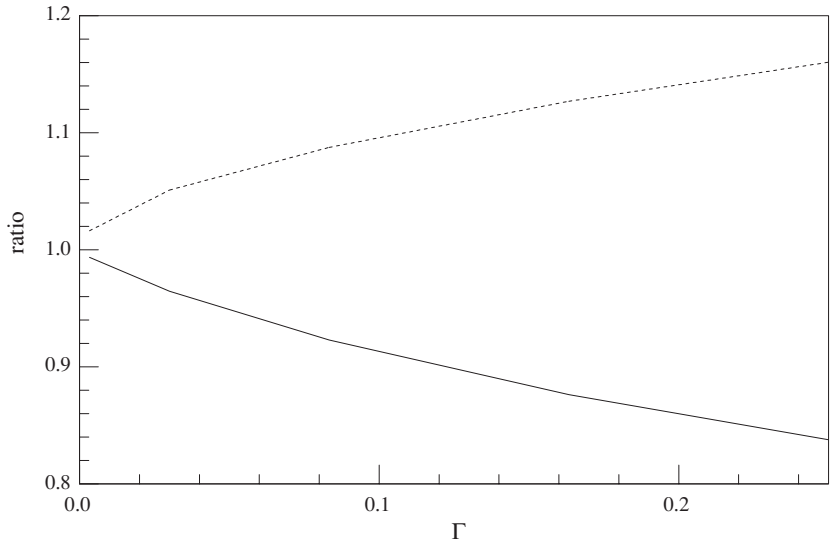

Figure 4. The ratio$_\Phi$ (the ratio of the matrix elements $\Phi_{if}^{\mathrm{AEIF}}$ and Φ_{if}^{ST} averaged over the microfields β), line ——; and the ratio$_\beta$ (the ratio of the mean values of the ionic microfields in the Coulomb and the Debye descriptions) line - - - -, versus the plasma parameter Γ.

probability distribution function $W_a^{(c)}(\beta, R_1)$.) The critical value β_c of the field strength results from the critical value of R_c for the distance R_1. In our opinion, the connection of R_c with the Weisskopf radius is inappropriate. We propose to take $R_c = 3a_0 n_i^2$ as the critical value, because for $R_1 < R_c$ the emitter would undergo ionization. Simultaneously, we find that the values of FWHM (obtained with using $\Phi_{if}^{\mathrm{AEIF}}$) of the H_α line calculated below are practically independent of R_c.

An appropriate measure of the contribution of $\Phi_{if}^{\mathrm{AEIF}}$ to the FWHM in relation to the values of FWHM calculated applying Φ_{if}^{ST} is the ratio

$$\mathrm{ratio}_\Phi = \frac{\int_0^\infty \Phi_{if}^{\mathrm{AEIF}} W_a^{(c)}(\beta)\,\mathrm{d}\beta}{\Phi_{if}} = \int_0^\infty f_a(\beta) W_a^{(c)}(\beta)\,\mathrm{d}\beta. \tag{23}$$

Another good measure of FWHM changes within the AEIF model, due to another description of the ionic microfield (in relation to the traditional theory), is the ratio

$$\mathrm{ratio}_\beta = \frac{\int_0^\infty \beta W_a^{(c)}(\beta)\,\mathrm{d}\beta}{\int_0^\infty \beta W_a(\beta)\,\mathrm{d}\beta}. \tag{24}$$

The values of both these ratios are presented in figure 4. It is clearly seen that two opposing mechanisms occur in the AEIF model. The changes of FWHM contributed by $\Phi_{if}^{\mathrm{AEIF}}$ produce a narrowing of the line, whereas changes caused by the probability distribution function of the ion microfield broaden the line. We performed calculations of the full line profiles in the quasistatic approximation as well as in the dynamic approximation for ions. The line profiles in the quasistatic approximation were calculated according to well-known formulae, e.g. [21, 53, 22]. In this approximation, the profiles of hydrogen spectral lines due to transitions from an initial (upper) i level (consisting of degenerate $i', i'', \ldots$ substates) to a final (lower) f level (consisting of f', f'', $\ldots$ sublevels) within the ST approximation, but including the corrected AEIF model of the electron–ion interactions, can be written

as follows:

$$P(\omega) = \frac{1}{\pi}\int_0^\infty \mathrm{d}\beta\, W_a^{(c)}(\beta)\,\mathrm{Re}\sum_{i'i''f'f''}\langle i'|\mathbf{d}|f'\rangle\langle f''|\mathbf{d}|i''\rangle \times \langle i'|\langle f'|\left[i\left(\omega - \frac{H_i(\beta)-H_f(\beta)}{\hbar}\right) + \Phi_{if}^{\mathrm{AEIF}}(\beta)\right]^{-1}|i''\rangle|f''\rangle. \tag{25}$$

The Hamiltonians $H_i(\beta)$ and $H_f(\beta)$ yield various initial i and final f energy states under the influence of the given ion field β. We calculated these profiles for H_α with and without the AEIF effect. In figure 2 we present the relative difference $\Delta\mathrm{FWHM_{ie}}$ for these profiles. Note that the ion–electron interactions, described by the corrected complete AEIF model, actually increase FWHM values in contrast to the originally reported [10] 25% decrease of the half width. Taking the ion dynamics into account, we obtain a still smaller AEIF contribution to the line profile as expected because of the reduced relative importance of the electron broadening.

In order to evaluate the influence of the AEIF model on the hydrogen line profile with the ion dynamics effect taken into account, we had assumed the statistical independence of the ion–emitter and electron–emitter interactions. With this simplifying assumption the autocorrelation function $C(t)$ of the line profile can be calculated as the product of the ionic $C_\mathrm{i}(t)$ and electronic $C_\mathrm{e}(t)$ autocorrelation functions

$$C(t) = C_\mathrm{i}(t)C_\mathrm{e}(t). \tag{26}$$

The ionic autocorrelation function was calculated in the pure dipole approximation by the computer simulation method described in [37, 44], whereas the electronic autocorrelation function has been taken in the impact approximation

$$C_\mathrm{e}(t) = \exp(-\Phi_{if}t). \tag{27}$$

We calculated the line profiles twice,

$$P(\omega) = \mathrm{Re}\,\frac{1}{\pi}\int_0^\infty C_\mathrm{i}(t)\exp(-\Phi_{if}t)\,\mathrm{d}t, \tag{28}$$

first taking the AEIF effect into account, and second neglecting this effect. In figure 2 we present the relative difference $\Delta\mathrm{FWHM_{ie}}$ for these profiles. As shown in this figure, inclusion of the ion-dynamic effect to the AEIF decreases the $\Delta\mathrm{FWHM_{ie}}$ values relative to the quasistatic approximation. Actually, the AEIF effect causes 4% increases in the FWHM values. Moreover, the approximation implied by equation (26) causes an about 10% erroneous increase of FWHM values. This is the cost of carrying out the calculation of the line profile taking into account simultaneously the AEIF (via the Φ_{if} operator) and the ion dynamics effects. Finally, the FWHM values of H_α,calculated with the AEIF model for the ion–electron interactions, are up to 15% larger then the FWHM values obtained by the FCSM method [6].

In order to check the accuracy of the approximation defined above, reference calculations were performed using the FCSM approximation without the assumptions yielding equation (26), and without the AEIF effect. These calculations were performed in the approximation described in [6]. Within this approximation, the dipole and the quadrupole interactions (for ions and electrons as well) are taken into account. The calculations were carried out up to the quadratic Stark effect for the microfield varying in time. In figure 5 this H_α profile calculated within FCSM is compared with our measured line profile (see section 4). These profiles agree excellently. From figure 5, we also see that the line profile in the approximation given by equation (28) (without AEIF effect) differs little from the profile in the FSCM approximation. Therefore, in our opinion, the approximation given by equation (26) is good enough for the examination of the relative importance of the AEIF effect.

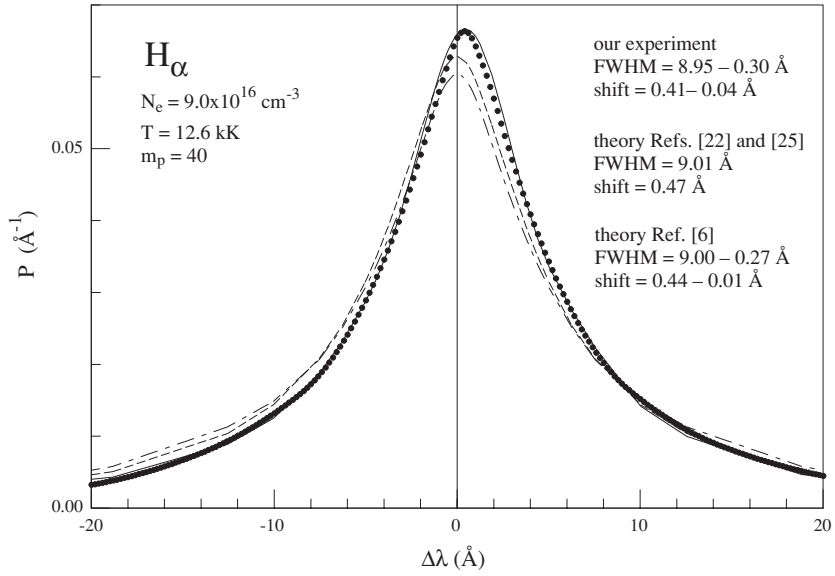

Figure 5. Comparison of calculated and measured line profiles of H_α. The line - - - - represents the calculations carried out within the dipole approximation according to equation (28) without AEIF effect, the line — · — with the AEIF effect, both including the ion dynamic effect. The line —— represents the line profile calculated using the full computer simulation method, as in [6], i.e. taking higher order interactions into account. The dots represent the results of our experiment. The profile calculated according to [22] (with the shift determined according to [25]) almost agrees with the solid line.

4. Arc experiment

4.1. Experimental set-up and radiation detection

Our aim here was the measurement of the H_α line profile formed in a hydrogen–argon plasma and the determination of the electron density N_e and temperature T. We also recorded spectral line intensities of H_β and ArI 4300 Å for the purpose of plasma diagnostics.

A wall-stabilized arc (Maecker–Shumaker type) with a channel diameter of 5.5 mm and length of 84 mm was used as the excitation source for atomic hydrogen and argon. We used the arc with a channel diameter larger than in the previous experiments [44, 66], in order to improve the homogeneity of plasma layers parallel to the arc axis. The arc channel is formed by a stack of ten water-cooled copper plates. Figure 6 shows a schematic of this arc. The wall-stabilized arc is operated at atmospheric pressure and at a current of 110 A. The central part of the arc column was operated in the mixture of argon and hydrogen, while the regions close to both electrodes were supplied additionally with very small amounts of argon in order to improve the stability of the discharge.

In figure 7 our experimental set-up is presented. This set-up is different only in some details from that described in [44, 66]; therefore, we restrict the following discussion to only a few essential remarks. The arc emission was observed in the end-on direction. The radiation emerging from arc (1) was imaged onto the 15μm wide entrance slit of the grating spectrometer PGS2 (6) using the concave mirror (3) with a large focal length (f = 730 mm) and the small diameter diaphragm in front of it (ϕ = 12 mm). It allows selecting the radiation originating from nearly homogeneous plasma layers parallel to the arc axis. The

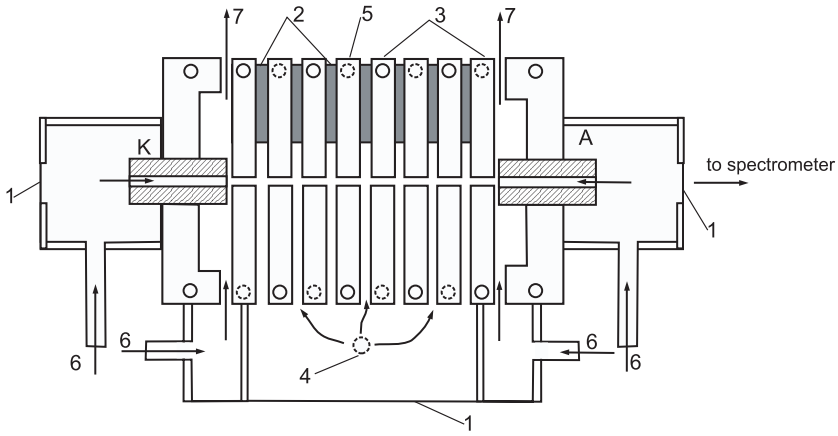

Figure 6. Schematic of the wall-stabilized arc. 1—quartz windows, 2—electrical insulator, 3—water cooling, 4—inlets of Ar+H_2, 5—copper rings, 6—Ar inlets, 7—outlets for the gas mixture.

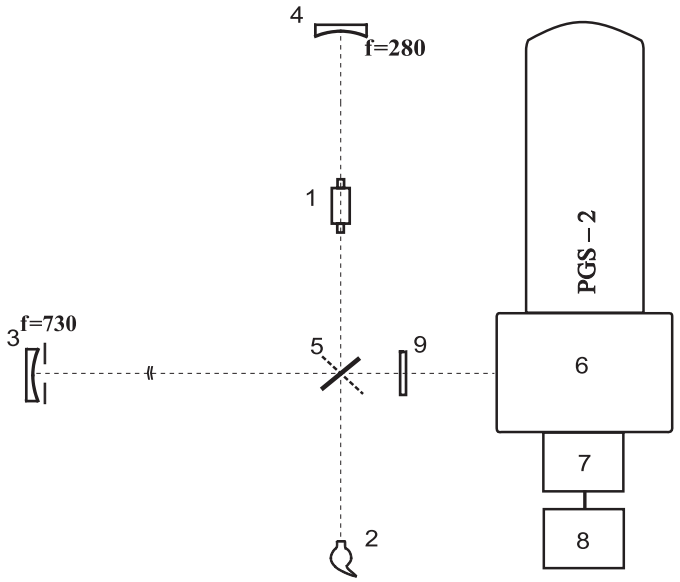

Figure 7. The scheme of the experimental set-up. 1—wall-stabilized arc, 2—tungsten strip lamp or Plücker-tube, 3 and 4—concave mirrors, 5—plane mirror, 6—grating spectrograph PGS-2, 7—computer, 8—OMA detector, 9—optical filter.

spatial resolution of our instrumentation was 0.25 mm. The homogeneity of individual plasma layers was controlled by the determination of the ratio between the FWHM width and peak separation of the H_β line. For homogeneous plasma layers the ratio should be 0.35 ± 0.01. The radiation was detected by using a two-dimensional optical multichannel analyser OMA4 (7) with regular pixel gaps of 0.019 mm. A reflecting grating with 1300 grooves mm^{-1} blazed at 5500 Å was used, yielding at the exit focal plane of the spectrometer dispersions of 0.063 and 0.067 Å/pixel for H_α and the ArI 4300 Å line, respectively.

Suitable filters (9) were placed in front of the entrance slit (see figure 7) in order to block the radiation below $\lambda = 3250$ Å and $\lambda = 6000$ Å for measurements of the ArI 4300 Å and

H_β lines, and for the H_α line, respectively. In this way we avoided possible interference of higher diffraction orders with the measured spectra around the ArI 4300 Å and H_β lines, and the studied H_α line.

The radiation emerging from the plasma column in the direction opposite to the spectrometer was reflected back by the concave mirror (4) to form an arc image in its own volume, thus almost doubling the intensities, see figure 7. The level of self-absorption was determined by comparing spectra recorded with and without the back-reflection. We reduced the amount of hydrogen flowing into the arc, in order for the self-absorption at the peak of H_α line not to exceed 5%.

By changing the angular position of the plane mirror (5), the emission of the tungsten strip radiation standard lamp or the low-pressure Plücker-tube discharge in hydrogen could be detected. In this manner, our arc emission was calibrated in intensity and wavelength.

4.2. Study of the measurement and plasma diagnostics

The apparatus noise was removed from our spectral recordings using the Fourier transform technique. This smoothing procedure is described in detail in [44]. Next, we performed self-absorption corrections. In the case of small self-absorption (relative to the Planck function), i.e. in optically thin and homogeneous plasma layers, the following relation is fulfilled, e.g. [67] page 196,

$$I(\lambda) = \epsilon(\lambda) l = -B(\lambda) \ln(1 - I_m(\lambda)/B(\lambda)), \tag{29}$$

where $I(\lambda)$ and $I_{\mathrm{m}}(\lambda)$ are total (spectral line and continuum) intensities corrected for self-absorption and measured, respectively; $\epsilon(\lambda)$ is the emission coefficient, $B(\lambda, T)$ is the Planck function, and l is the length of the plasma column. For the intensity $I(\lambda)$ we determined the level of the continuum according to a procedure described in the previous [44]. Namely, on the basis of theoretical premises, we assumed that the wings of the spectral lines exhibit power-law shapes. The continuum was approximated by a function depending linearly on wavelength. With such a function, the distribution of the spectral intensity—in wavelength intervals corresponding to the spectral line wings—can be written in the following form:

$$\begin{aligned} I(\Delta\lambda) &= a_{\mathrm{v}}|\Delta\lambda|^{b_{\mathrm{v}}} + a_{\mathrm{c}}\Delta\lambda + b_{\mathrm{c}} \qquad \text{for the } \textit{violet} \text{ wing,} \\ I(\Delta\lambda) &= a_{\mathrm{r}}(\Delta\lambda)^{b_{\mathrm{r}}} + a_{\mathrm{c}}\Delta\lambda + b_{\mathrm{c}} \qquad \text{for the } \textit{red} \text{ wing,} \end{aligned} \tag{30}$$

where $\Delta\lambda = \lambda - \lambda_0$, with λ_0 being the wavelength of the unperturbed line. The parameters for the wings ($a_{\mathrm{v}}, b_{\mathrm{v}}, a_{\mathrm{r}}, b_{\mathrm{r}}$) as well as for the continuum ($a_{\mathrm{c}}, b_{\mathrm{c}}$) were determined by a least-squares-fitting procedure on the basis of spectral intensities $I(\lambda)$ corresponding only to the outer parts of the line profile, for which the signal did not exceed 1/8 of the maximum spectral line intensity. By subtracting the continuum intensity $I_{\mathrm{c}}(\lambda)$ from the total intensity $I(\lambda)$, we obtained intensity distributions of the spectral lines $I_{\mathrm{l}}(\lambda) = I(\lambda) - I_{\mathrm{c}}(\lambda)$ for H_α, H_β and ArI 4300 Å. The relationship between the line profile $P(\Delta\omega)$ and the spectral line intensity distribution $I_{\mathrm{l}}(\lambda)$ can be written approximately [68] as

$$I_{\mathrm{l}}(\Delta\omega) = I_0(\omega_0)(1 + \Delta\omega/\Delta\omega_0)^4 \exp(\hbar\Delta\omega/kT) P(\Delta\omega). \tag{31}$$

The power factor represents changes of the transition probability (power 3) and of the photon energy (power 1) as a function of $\Delta\omega$. The exponential factor represents approximately the population change of the upper energy level. Such form of the exponential factor may be appropriate only for the quasistatic contribution. So, the line profile $P(\Delta\omega)$ has been corrected for the so-called trivial asymmetry. This analysis of the measurements was performed for the three spectral lines H_α, H_β and ArI 4300 Å for five independent measurements, results of which (lines profile and integral emission coefficient) were averaged in the case of each line.

This average experimental H_α line profile is presented in figure 5. The values of FWHM width and shift and their accuracies are indicated on this figure.

The Plücker-tube served as a light source for the experimental determination of the spectral width of the instrumental profile, and as a standard for the wavelength calibration. We assumed that the width of the H_α line emitted from the Plücker-tube is not greater than the apparatus profile. This profile can be well approximated by a Gaussian of full width at half maximum (FWHM) about 0.12 Å. This last value is significantly smaller than the accuracy in the measurement of FWHM widths of the line profile P in our plasma. Therefore, we neglected the influence of the apparatus profile on the line profile P. We accepted the maximum of that Gauss profile as the wavelength λ_0 of the isolated atom. The accuracy of this λ_0 determination should be within one half of one pixel, i.e. about 0.03 Å.

We first determined the electron density N_e using the FWHM of the H_β line; we obtained about $9 \times 10^{16}\,\mathrm{cm}^{-3}$. In [69] it is shown experimentally that in the pure argon plasma, produced in a wall-stabilized arc, for $N_e > 6 \times 10^{16}\,\mathrm{cm}^{-3}$ the requirements of local thermodynamic equilibrium (LTE) are fulfilled. (Adding a small amount of hydrogen to the argon plasma improved the LTE conditions.) Therefore, to determine N_e and T by a method independent of Stark line profiles, we carried out the plasma diagnostics using the LTE model and taking the integral emission coefficients of the H_β and ArI 4300 Å from the experiment. The values of N_e and T thus obtained are also gathered in figure 5. We observe excellent agreement of the calculated line profile (Stark and Doppler) with the measured one.

In our opinion, the principal requirement for such a comparison is to have a reliable experimental line profile, i.e. a line profile formed in a homogeneous plasma layer of small optical depth.

5. Comparison of previous experiments with calculations

As is well known, homogeneous and optically-thin plasmas are most suitable for reliable line-profile measurements. However, such ideal conditions are not achievable at high densities, leaving one with the necessity of critical assessment of systematic errors. As can be seen from figure 4 of [13], not even the background intensity from krypton with 4% hydrogen is completely optically thin near H_α. Moreover, the apparent continuum slope is not consistent with the plasma conditions inferred from absolute intensities of optically-thick KrI lines in the infrared, single wavelength (3.39 μm) laser-interferometry, and from radial scans of the (optically-thin) continuum intensity at short wavelengths (3200 Å). Evidently self-absorption corrections were performed as if the plasma was radially homogeneous (which seems very unlikely in view of the radial distributions observed in an earlier helium flash-tube experiment [45]), and the corrected spectra were then Abel-inverted. (These procedures should actually have been 'coupled', i.e. have been calculated iteratively. This would result in narrower profiles.) Since the KrI line emission probably occurs mostly in the outer region, the actual temperature in the central region may well be higher. The line-profile corrections are clearly unreliable, since the radiance values in figures 4 and 5 of [13] at the peak of H_α suggest sums of (density-scaled) continuum intensities from figure 4 and line intensities from figure 5 at least equal or even exceed the Planck intensity at the quoted temperature. The measurements may well have been compromised further by optical distortions in the walls of the 3 mm inner diameter tube, which would tend to smooth out the actual radial distributions. Neglecting profile corrections accounting for contributions from the outer regions therefore is quite questionable. Moreover, evidently a constant continuum slope was assumed for subtracting the background emission near H_α, rather than a measured background determined from pure krypton discharges. If the latter procedure had been used, more likely than not

the spectrum in the 6000–7000 Å region would not have been entirely continuous, but would have shown the six KrII lines with estimated intensities $I \gtrsim 100$ in Striganov and Sventitskii's tables [46] (if one includes the line at 5992 Å). At least at the higher temperatures, i.e. $T \lesssim 2 \times 10^4$ K, these lines are estimated to have about 5% (integrated) line intensities relative to H_α intensities from the 4% admixture (assuming LTE and KrII oscillator strengths of $f = 0.05$ from the Cowan code [47]). Moreover, from measured Stark widths of lines from the same or similar upper levels [48], the expected FWHM widths of these lines are $\lesssim$30 Å at the highest density in [13]. The strongest of these KrII lines, at 6420 Å [46], is probably responsible for the observed hump around $\lambda = 6400$ Å on the blue wing of the H_α profile shown in figure 5 of [13]. It can easily cause a blue shift of ∼5 Å in the best-fit (symmetrical) profile, i.e. a systematic error in the shift measurements twice larger than the error given in [13]. Two of the tabulated KrII lines, at 6511 and 6570 Å [46], are probably blended with the H_α line core, possibly even reducing the line width of the composite profile by $\lesssim$5%. The remaining three lines are too far from H_α to cause significant errors, but seem to be noticeable in figure 5 of [13] at 6764, 6303 and 5992 Å [46], albeit very near the noise level. (Note that these well-separated lines have substantially smaller estimated intensities [46] than the 6420 Å KrII line, the 5992 Å line being the next strongest line.)

According to various measurements [48], all KrI lines in the wavelength range of interest should be very broad, their upper levels being close to the Inglis–Teller limit [22, 23, 49]. Two of the most intense KrI lines, at 6456 and 6421 Å [46], may well contribute to the hump on the blue wing of H_α mentioned above. This strengthens the case for a significant systematic error in the measured shifts in the flash-tube experiment [13] also at lower temperatures, where the KrII 6420 Å line would be less intense. Further errors are of course to be expected from inhomogeneities and absorption corrections. There are no intense KrI lines listed [46] near the H_α line core, so that at lower temperatures one would not expect a narrowing as suggested above due to the blend with KrII lines. In our opinion, the estimated uncertainties in the N_e and, especially, T determinations are too optimistic. Errors originating from self-absorption corrections, large uncertainty (reaching 100%) of the continuum levels (see figure 7 in [50]), and the lack of direct dynamical pressure measurements do not allow for reliable diagnostics. All of these considerations suggest a careful reinterpretation of the experimental results in [13].

To summarize, due to systematic errors caused by the inhomogeneity of the plasma in measurements of the H_α line profile, as well as due to errors in the procedure used to allow for the self-absorption and blending (by Kr lines), the FWHM values measured in [13] are more likely than not systematically overestimated, whereas measured values of the red shift are underestimated. Actually, the results of the earlier experiments [51, 15] are probably more reliable. These experiments were performed with argon and (trace) hydrogen plasmas produced in flash-tubes as well. The continuous spectrum of Ar plasmas is known with greatly better accuracy than for Kr plasmas. Furthermore, in the experiments [51] and [15] the H_α profile had been corrected for the blending, but well resolved, lines of ArII.

In [52] an experiment was described, which is very similar to experiments with the flash-tube [13, 51, 15]. In this other experiment [52], pure hydrogen plasmas had been produced in a capillary (of 12 mm length and 4 mm diameter) by the electrical discharge of a condenser battery of 1800 μF capacity. These authors of [52] measured (red) shifts of the H_α line for electron densities in the range $N_e = (0.2\text{–}1.0) \times 10^{18}\,\mathrm{cm}^{-3}$ at temperatures in the range $T = (24\text{–}26)$ kK. This range of physical conditions approaches the physical conditions in the flash-tube experiment [51]. However, in [52] the measured shifts are systematically greater by about 1 Å than the shifts reported in [51]. In our opinion, the results in [52] are more reliable, because in pure hydrogen plasmas the continuum near the H_α line is unambiguously

Table 1. Experimental FWHM widths from the flash-tube experiment [13] and their ratios to calculated widths quoted in [13] using Oks' theory and ST (standard theory[a] [22, 21] and FCSM (full computer simulation method [58]) widths. (a) Initial gas pressure 600 Torr, (b) 400 Torr and (c) 300 Torr.

N_e		FWHM	Width ratios		
(10^{18} cm^{-3})	T (K)	(Å)	Oks	ST	FCSM
		(a)			
1.10	13 350	64	1.07	1.10	1.24
1.70	14 180	78	1.00	1.01	1.08
2.20	14 900	90	0.98	0.96	1.05
2.60	15 500	101	0.99	0.95	1.05
3.30	16 230	116	1.00	0.92	1.03
3.90	17 100	126	1.02	0.91	1.00
4.40	18 080	145	1.11	0.95	1.04
		(b)			
1.25	14 400	64	0.98	1.00	1.13
1.80	14 450	78	0.98	1.00	1.04
2.25	16 410	88	0.97	0.93	1.01
2.40	17 420	97	1.00	0.96	1.06
3.00	17 880	113	1.04	0.97	1.07
3.50	18 640	122	1.03	0.93	1.13
3.70	19 600	135	1.11	0.99	1.08
		(c)			
1.40	13 810	64	0.94	0.96	1.05
1.60	14 700	74	0.96	0.97	1.08
2.10	15 600	80	0.91	0.89	0.96
2.40	16 470	96	0.99	0.95	1.05
2.90	17 450	108	1.00	0.94	1.05

(a) Including complete interference term and allowing for inelastic electron collisions.

determined, in contrast to the continua in argon and, especially, in krypton plasmas, both with small hydrogen admixtures [13, 51, 15]. On the other hand, according to the width comparisons in table 1 of [13] and in table 1 here, which lists the ratios of measured and some calculated widths, the measured widths agree with both sets of calculations to better than 10%, i.e. within estimated experimental errors. The statement in the abstract of [13] of 'rms deviation from the most probable experimental widths' being 46% larger for the previous calculations versus 'Oks' widths' is therefore quite misleading. Actually, were the blends with KrII lines at the higher temperatures (and densities) allowed for, a reanalysis might even favour the old calculations [21–23]. Thus, the concluding statement in the abstract of [13] of 'further proof of some new warm-dense matter effects' is certainly not supported by these width comparisons. That experimental errors are probably larger than estimated in [13] is also indicated by the apparent lack of any density dependence of the measured widths (64 Å) at the lowest densities for the various fill pressures, whereas the classical $N_e^{2/3}$ density scaling would suggest, say, 54, 59 and 64 Å, respectively. This would then give 1.05 for all three FCSM [58] ratios at the lowest N_e values. Improved computer simulations (including quadrupole interactions and quadratic Stark effects) [44] result in 2% to 7% smaller widths than in [58] at densities 1.1×10^{18} and 4.4×10^{18} cm^{-3}, respectively, i.e. slightly larger width ratios than in the last column of table 1. Ion-dynamical effects, which were neglected in the original ST calculations, should only be 1–2%, judging by the weak dependence on the reduced radiator–perturber mass [58]. They were partially accounted for in the AGT calculations by extending the mostly

Table 2. Measured and calculated H_α line shifts for the same conditions as in table 1. The column labelled 'Oks' gives the calculated shifts from [13], 'Griem' those from [24] and [25], i.e. including the blue shifts from quadrupole interactions, etc (see text), and the last column the shift after correcting for the Debye screening.

N_e (10^{18} cm^{-3})	T (K)	Line shifts (Å)			
		Measured	Oks	Griem	Corrected
		(a)			
1.10	13 350	4.8 ± 0.7	4.8	$7.0 - 1.4 = 5.6$	5.0
1.70	14 180	6.6 ± 1.0	7.2	$10.7 - 2.1 = 8.6$	7.7
2.20	14 900	8.9 ± 1.3	9.5	$14.2 - 2.8 = 11.4$	10.2
2.60	15 500	11.6 ± 1.7	11.4	$17.0 - 3.3 = 13.7$	12.3
3.30	16 230	14.2 ± 2.1	14.6	$21.8 - 4.2 = 17.4$	15.8
3.90	17 100	16.8 ± 2.5	17.0	$26.3 - 4.9 = 21.4$	19.0
4.40	18 080	19.8 ± 2.9	19.5	$30.1 - 5.6 = 24.5$	22.0
		(b)			
1.25	14 400	5.2 ± 0.8	5.5	$8.0 - 1.6 = 6.4$	5.7
1.80	15 450	6.7 ± 1.0	7.8	$11.6 - 2.3 = 9.3$	8.3
2.25	16 410	8.7 ± 1.3	10.0	$14.8 - 2.9 = 11.9$	10.6
2.40	17 420	10.4 ± 1.5	11.0	$16.1 - 3.0 = 13.1$	11.8
3.00	17 880	12.3 ± 1.8	13.6	$19.8 - 3.8 = 16.0$	14.3
3.50	18 640	14.3 ± 2.1	16.1	$23.5 - 4.4 = 19.1$	17.1
3.70	19 600	15.8 ± 2.3	17.4	$25.2 - 4.7 = 20.5$	18.4
		(c)			
1.40	13 810	4.9 ± 0.8	5.9	$8.8 - 1.8 = 7.0$	6.3
1.60	14 700	6.3 ± 0.9	7.1	$10.4 - 2.0 = 8.4$	7.6
2.10	15 600	7.8 ± 1.2	9.2	$13.6 - 2.7 = 10.9$	9.8
2.40	16 470	9.9 ± 1.5	10.8	$15.9 - 3.0 = 12.9$	11.6
2.90	17 450	11.5 ± 1.7	13.1	$19.4 - 3.7 = 15.7$	14.1

non-perturbative treatment of electron collisions to fast ions, i.e. using the rather inappropriate assumption of adiabatic, binary collisions. This is clearly incorrect for the central, unshifted component, as already discussed in section 2.

The Debye screening effect on the AGT dipole-ion-electron shift (DIES) remains more or less an academic question, averaging out to zero anyway after summing over symmetrically displaced Stark components. (This is no longer true, if one allows for corrections of the perturber distribution [25].) For any given Stark component, however, it increases its Stark shift and therefore also the line width. In the notation used for isolated lines [22, 23, 59] these additional shifts are proportional to the characteristic $b(z_{\min}) = \int_{z_{\min}}^{\infty} B(z)\,\mathrm{d}z/z \approx \pi/2$ functions, z being a dimensionless variable characterizing the electron collision, and $\pi/2$ the so-called high-temperature (small level splitting) limit, which was evidently used in equation (1) of [20]. To account for screening, the upper limit is replaced by $z_{\max}$, equivalent to the subtraction of $b(\omega/\omega_p)$. For $z_{\max} \lesssim 1$ and $z_{\min} \ll 1$, one finds $b(z_{\max}) \approx (0.5 \pm 0.1) z_{\max}$ in agreement with an estimate given already in the original paper [38] on these shifts. From the expression for $z_{\max}$ also given there, one then finds a reduction factor of $\lesssim 0.25$ for the DIES contributions, in contrast to a statement in [60]. Note that the larger reduction factor there, $6.653\left(n^2 a_0 N_e^{1/3}/\pi\right)^{1/2}$, does not appear on page 1059 of [38], also in contrast to a statement in paragraph 2 of [60]. Another estimate of the Debye reduction factor made in [27], using a $z_{\max}$ value corresponding to the HWHM, gave an even smaller value, namely $\lesssim 0.1$.

As for the shift comparisons in table 2 of the flash-tube paper [13], the calculated shifts in the last column are apparently the electron-collisional shifts from [25], table I. However,

as discussed in this and a preceding paper [24], these electron-induced red shifts must be combined with blue shifts caused by ion–atom quadrupole interactions [38], quadratic Stark effects and the so-called trivial corrections (from the ω^4 factor in the line intensity formula, etc), before comparison with measurements. As can be seen, e.g. from table III of [25], this results in an about 20% reduction of the calculated shifts. Moreover, equation (10) of [24] suggests that the Debye screening reduces the $n' \neq n$ electron collisional shifts there by $\lesssim$10%, estimated by subtracting $b(\omega/\omega_p)$ from $b(z_n)$ in this equation. A slightly smaller reduction would be obtained by using the equation on page 321 of [22], proposed for the Debye corrections of the tabulated Stark widths and shifts of the so-called isolated lines from nonhydrogenic neutral atoms. (That neglecting Debye screening for electron densities $\lesssim 2 \times 10^{18}$ cm^{-3} is appropriate had been noticed already in the first calculations [59] of the Stark broadening parameters for neutral helium lines.) After these corrections (see table 2 here), the 'discrepancies of up to 76%' in the abstract of [13] become up to 20%, by which the measured shifts in the flash-tube experiment are smaller than those calculated previously [25]. The corresponding deviations are $\lesssim$1 Å at lower densities and $\lesssim$2.5 Å at the highest densities, i.e. not significant given the quoted experimental errors and the blend with the KrII 6420 Å line. We note here that the improved computer simulations [44] do yield blue shifts from ion–atom interactions consistent with the so-called ELC (experimental line centre) shifts in [24], but show that best-fit Lorentzians are more blue-shifted by factors 1.3–1.5. Corresponding corrections would actually reduce the deviations between measured and calculated shifts. In any case, there is again no substantial experimental evidence for 'warm-dense-matter effects.' (Note, finally, that the quadrupole effects on the distant line wings cause an asymmetry which would cancel the blue shift were one to integrate the first moment of $L(\omega)$ over the frequency displacement from minus to plus infinity.)

More important in view of the possible systematic errors is, however, a comparison with the recent shift measurements [17] in the Bochum gas-liner pinch experiment. (In contrast to the widths determined in this recent experiment (13 of [13]), these shifts had been ignored in [13].) Table 1 of [17] contains measured widths and shifts from $N_e \approx 0.5$–2.5×10^{18} cm^{-3} at temperatures $kT \approx 5-10$ eV. For example, measured red shifts are 4.8 and 12.3 Å at $N_e = 0.99$ and 1.96×10^{18} cm^{-3} and temperatures 7.1 and 8.4 eV, respectively. These temperatures are higher than those assumed in the original calculations [24, 25], but straightforward calculations of the dominant $\Delta n = 1$ electron-collisional shifts using equation (10) of [24] suggest that these are peaking near 5 eV, so that multiplying the largest $\Delta n \neq 0$ value in table I of [25] by a factor of 1.2 should give a good estimate for the $\Delta n \neq 0$ contributions, i.e. 7.1 and 14.1 Å, respectively. Adding the $\Delta n = 0$ electron contributions of about 0.7 and 1.3 Å (again extrapolated from table I of [25]) and subtracting the ion-quadrupole, etc., shifts from table III of [25] of 1.5 and 2.9 Å, the 'conventional reference' thus gives red shifts of 6.3 and 12.5 Å. With the Debye corrections also for the $\Delta n \neq 0$ contributions, these calculated shifts become 5.8 and 11.3 Å, 20% larger or $\lesssim$2% smaller than the measured shifts [17]. A corresponding calculation for the lowest density and temperature case in [17] gives red shifts of 3.2 and 3.0 Å, without or with the Debye correction. The measured value was 2.6 Å, i.e. again in satisfactory agreement. (For this case the reply [60] claims 'up to a factor of 2' disagreement, probably for the reasons mentioned above and errors from extrapolating table I of [25] to higher temperatures.) Given experimental errors of $\approx$10% and similar uncertainties in the calculations, these remaining deviations are not significant.

For better transparency, the measured FWHM widths and the measured shifts are compared here with calculated values in six figures, from 8 up to 13. In figures 8 and 9, the experimental FWHM widths and shifts for the flash-tube plasma [13, 51, 15] and for the capillary plasma [52] are compared with calculations [6, 22, 57, 58]. At the beginning

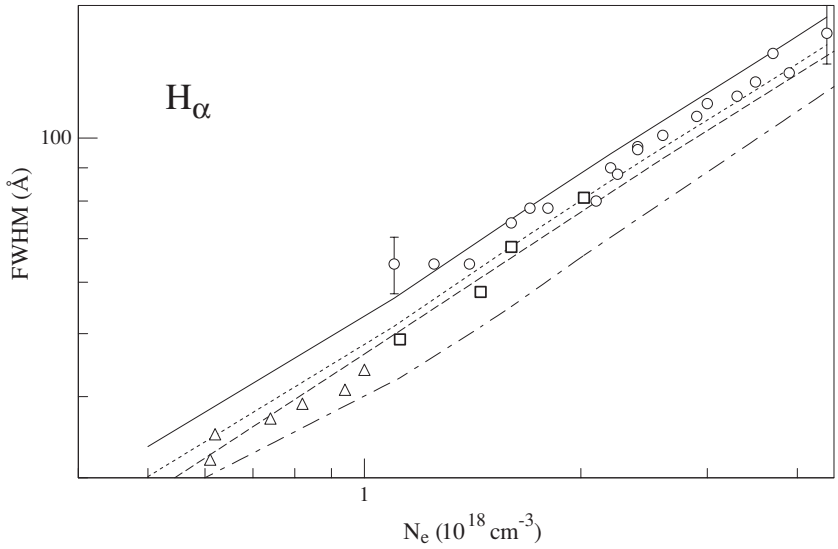

Figure 8. Widths of the H_α line versus electron density from flash-tube experiments: ○, [13] Kr+H plasma; △, [51] Ar+H plasma; □, [15] Ar+H plasma. Theoretical results calculated for plasma conditions in flash-tube experiments: ——, [22]; – – –, [6]; — · —, [57]; - - - -, [58].

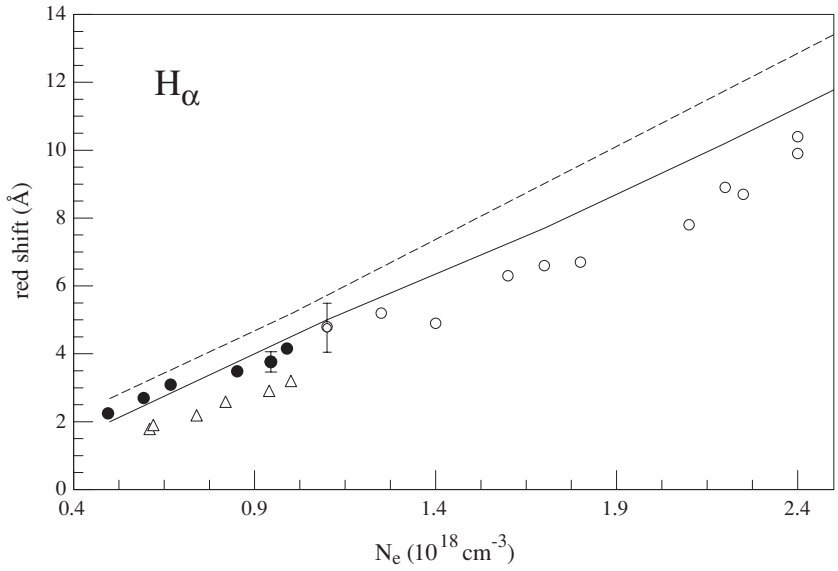

Figure 9. Shifts of the H_α line versus electron density. (Symbols are as in figure 8.) Additionally, the symbols ● represent experimental results [52] for pure H plasmas generated by an electrical discharge in a capillary. The lines ——corresponds to calculations [24] and [25] with the correction described here, – – – to [6].

of this section we already noted that experimental values of FWHM (marked in figure 8 as open circles [13]) are probably overstated. The experimental situation [13] is indecisive, since an earlier flash-tube experiment [51] in argon with small hydrogen admixtures yielded 44 Å for the width of H_α at $N_e = 10^{18}$ cm^{-3}, corresponding to 47 Å at the lowest density

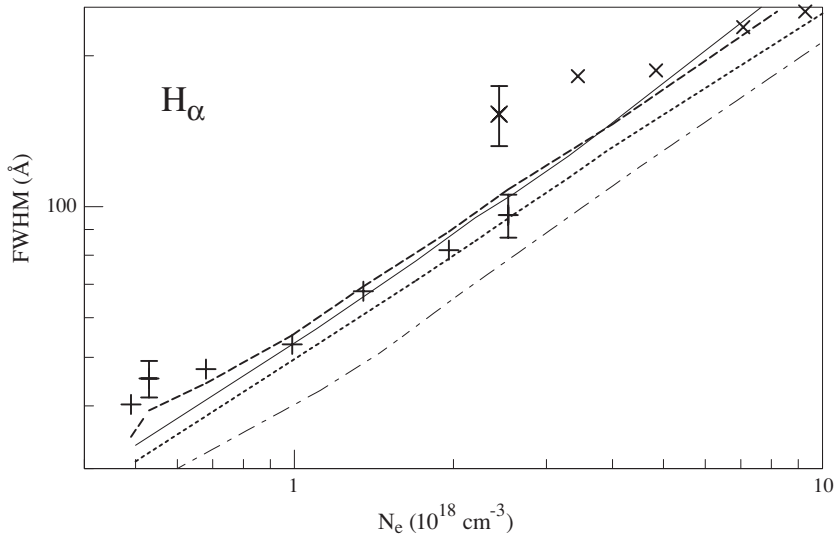

Figure 10. Width of the H_α line versus electron density. The symbols correspond to results from gas-liner pinch experiments: +, [17]; ×, [18]. The curves represent theoretical results calculated for plasma conditions in these experiments: ——, [22]; – – –, [6]; — · —, [57]; - - - -, [58].

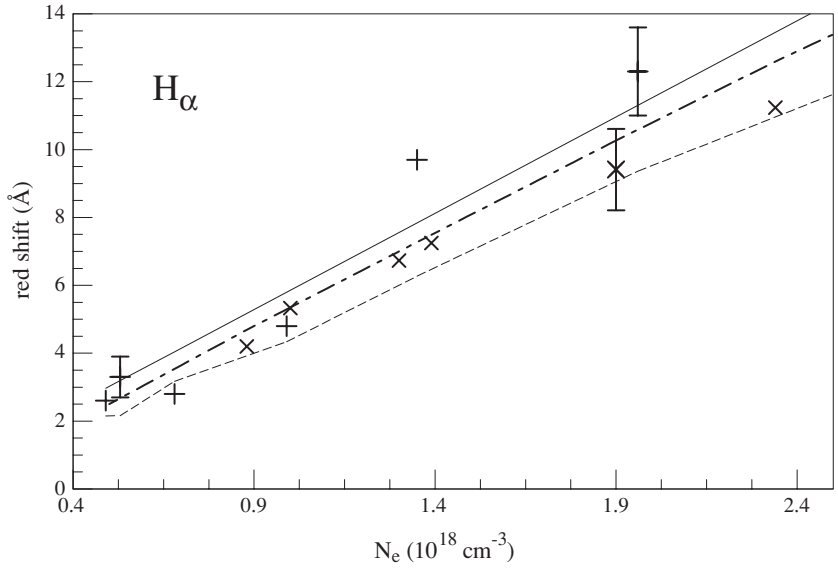

Figure 11. Shift of the H_α line versus electron density. Symbols and curves mean the same as in figure 10, with the exception of the — · — curve, which represents theoretical results obtained using the Green function technique [18].

$N_e = 1.1 \times 10^{18}$ cm^{-3} in [13], where it was measured as 64 Å. These large errors in width determinations imply large uncertainties also for the line shifts determined in [13] (not to mention those in [12, 14] where resonance broadening may well contribute to the width, but of course not to the shift of H-alpha). This is clearly seen from the inconsistency of the measured shifts in a pure hydrogen capillary plasma [52] (indicated as full circles in figure 9)

and measured shifts in an argon–hydrogen (minority) flash-tube plasma [51] (indicated as triangles in figure 9). Taking the above observations into account, we state that the measured FWHM values are predicted best by the FCSM [6], whereas the shifts agree best with ST [24, 25] together with the corrections for the Debye shielding, etc, discussed above.

In figures 10 and 11 the experimental results for FWHM widths and shifts for the gas-liner pinch [17, 18] are compared with calculations [6, 22, 57, 58]. (We would like to explain that the theoretical FWHM values [58] should be considered as approximate, because they correspond to a temperature of 40 kK, i.e. to the highest one in the tables [58], whereas temperature values in the experiment amount to about 100 kK. These high temperature values cannot be extrapolated with confidence because the FWHM-temperature dependence at a fixed N_e value is not monotonic.) In figure 10 we clearly see that measurements in the so-called first Bochum experiment [18] for $N_e \geqslant 2 \times 10^{18}$ cm^{-3} are affected by some systematic error, and therefore they are not included in the measurement–theory comparisons. Consequently, the FWHM values measured in the gas-liner pinch plasma are best predicted by the FCSM in [6]. In the case of the line shifts, all the three theories (Griem [24, 25] with the corrections here, Günter and Könies quoted in [18] and Olchawa [6]), predict values within experimental errors. The smallest rms deviation is obtained using [24, 25], after correcting for Debye shielding.

6. Conclusions

We have shown that if optimal circumstances are fulfilled for measurements of line profiles, i.e. if the plasma is optically thin and homogeneous, then experimental profiles agree excellently with calculated ones from the full computer simulation method (FCSM) [6, 44] and from the standard theory (ST) [22, 24, 25], see figure 5.

In figures 12 and 13 the measurements of the flash-tube plasma and of the gas-liner pinch plasma are compared. In these figures results of the theoretical calculations agreeing best with the measurements are also presented. In figure 12 for the FWHMs widths these are the calculations obtained by Olchawa [6], whereas in figure 13 for (red) shifts they are the calculations by Griem (i.e. [24, 25] with corrections here). We showed in sections 2 and 5 that the values of the FWHM widths in krypton–hydrogen flash-tube plasmas [13] (marked as open circles in figure 12) are systematically overestimated by about 25%. After such correction widths from the gas-liner pinch would actually be larger than those from the flash-tube plasma, i.e. at fixed electron density the FWHM values are larger at the higher temperatures. Similarly, for the shifts (marked by open circles in figure 13) we proved that they were underestimated in the flash-tube plasma [13, 51, 15].

In figures 12 and 13 the results of an underwater laser spark experiment [12, 14] and of the so-called Oks' theory in [13, 14] are not included, because in both cases the results are unreliable. As already mentioned in [29], the conclusions drawn on the basis of the experiment [14, 12] are obviously flawed, because the plasma conditions inferred from the spectroscopic measurements there would correspond to a compression to about 1.5 times of the normal water density, not to mention that the neutral hydrogen density would be high enough for resonance broadening [23] to dominate over the Stark broadening.

In this paper, in section 3, we have shown that in the basic work [19] (i.e. in the so-called generalized theory) un-physical approximations were applied, as well as in all subsequent calculations based on GT [9, 11–13, 60–63]. In section 3 it is shown that the so-called acceleration of electrons by the ion field (AEIF) effect [10] is no new effect but only an over-simplified model including algebraic errors, relative to traditional theory (ST, FCSM, etc), of the ion–electron interactions. Corrected, but still not devoid of faults, the AEIF model yields about 4% increase of the half width of H-alpha (worsening the agreement with

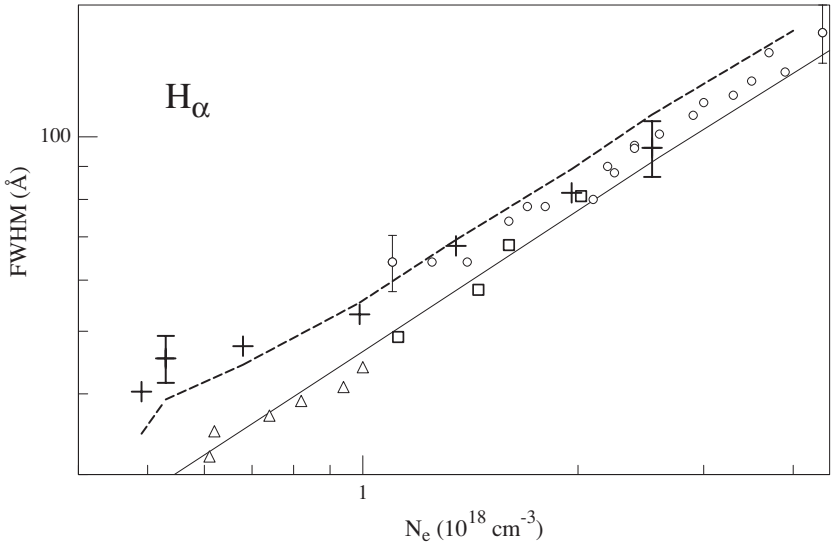

Figure 12. Comparison of FWHM widths of the H_α line from flash-tube experiments with those from gas-liner pinch experiments. The symbols are as in figures 8 and 10. However, the curves correspond to calculations according to [6] performed for plasma conditions: —— in flash-tube experiments; – – – in gas-liner pinch experiments, respectively.

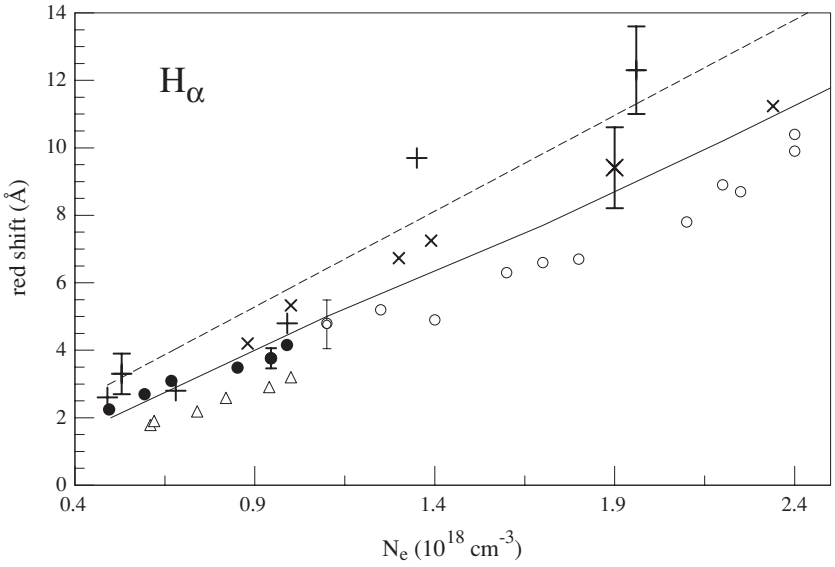

Figure 13. Comparison of shifts of the Hα line from flash-tube experiments with those from gas-liner pinch experiments. The symbols are as in figures 9 and 13. However, the curves correspond to calculations according to [24] and [25] with the correction described in this paper performed for plasma conditions: —— in flash-tube experiments; – – – in gas-liner pinch experiments.

experimental data), in contrast to the original [10] 25% decrease of the half width. Additionally, approximations implied by equation (26) cause an about 10% erroneous increase of the FWHM values. This is the cost of carrying out the calculation of the line profile taking into account

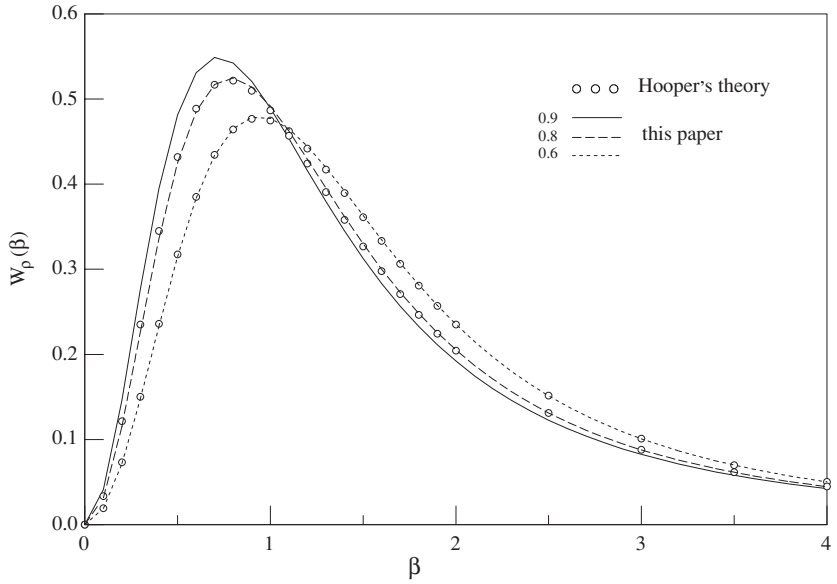

Figure 14. The electric microfield distributions function $W_a(\beta)$ at a neutral point as a function of the reduced electric field strength for perturbing ions of charge equal to 1 and for different screening parameters. The lines represent the results obtained in this paper; the symbols represent the results from [41].

simultaneously the AEIF (via the Φ_{if} operator) and the ion dynamics effects. Thus, total increases of FWHM values calculated with the inclusion of the AEIF effect, relative to those obtained using FCSM, amount to about 15%. For the physical conditions in figure 5, the AEIF model yields 10.3 Å for the FWHM width; such increases of FWHM values would worsen the agreement with experimental data.

To summarize, we have shown that existing theories describe the experimental values of FWHMs and shifts of the H_α line (at high electrons densities, for plasma parameters $\Gamma \leqslant 0.25$) very well, and there is neither theoretical nor substantial experimental evidence for the existence of the new 'warm-dense matter effects' claimed in [13] and [12, 14], nor in the recent reply [60] to one of the earlier comments [28]. This conclusion is consistent with shift-to-width ratios of about 0.1 in a laser-driven pressure cell at densities up to $\sim 2 \times 10^{19}$ cm^{-3} [16], a case for which the Debye shielding of $n' \neq n$ electron–dipole interactions is very important. Figure 2 in [16] suggests that, overall, also shifts increase less than linearly with the density, but are sensitive to temperature. (See, e.g. the calculated shifts, corresponding to FWHM widths of $\lesssim$230 Å, which are as much as a factor 1.3 larger at gas-liner pinch temperatures [17] compared to those in the flash-tube experiment [13].) This is consistent not only with the Green function technique [64] calculations by Günter and Sorge quoted in [16], but also with ST calculations [24, 25], corrected for the Debye screening as discussed here, and with computer simulations [6, 44] including quadratic Stark effects and electric field gradients.

Acknowledgments

Suggestions by S Alexiou, G Grabowski, H-J Kunze, and T Wujec are gratefully acknowledged, as is the partial support by the US National Science Foundation.

Appendix. Microfield distribution function

In the experiment [13] values of the electron density N_e and temperature T were obtained leading to screening parameters $a = R_0/D$ greater than 0.8. The numerical values of microfield distribution functions $W_a(\beta)$ at a neutral point for screening parameters $a > 0.8$ are missing in the literature [39–41]. In order to avoid extrapolation, we calculated the numerical values of the $W_a(\beta)$ function for $a = 0.9$. The calculations were carried out within the Mozer–Baranger approximation [39]. Figure 14 represents our results in comparison with results by Hooper [41], to assess the accuracy of our approximation and of the numerical code. We see that in the range $a \leqslant 0.8$ no discrepancy between our and Hooper's [41] values occurs; therefore, we conclude that our approach is sufficiently accurate also in the case of the $W_{0.9}(\beta)$ function. We see furthermore that the discrepancy, reported in [41], between Hooper's $W_a(\beta)$ values [41] and Mozer–Baranger's [39] are not caused by differences between models but by numerical inaccuracies in [39].

Similarly, we calculated the numerical values of functions $W_a^{(c)}(\beta)$ for the Coulomb ion microfield. The shape of the functions $W_a^{(c)}(\beta)$ are also similar to the functions $W_a(\beta)$. The functions $W_a^{(c)}(\beta)$ agree very well with Hooper's results [43] for the so-called high-frequency electric microfield, which also was calculated for the Coulomb field.

References

[1] Grabowski B, Madej J and Halenka J 1987 *Astrophys. J* **313** 750
[2] Madej J and Grabowski B 1990 *Astron. Astrophys.* **229** 467
[3] Griem H R 2000 *Contrib. Plasma Phys.* **40** 46
[4] Griem H R 2001 *Contrib. Plasma Phys.* **41** 223
[5] Halenka J, Olchawa W, Grabowski B and Gajda F 2002 *J. Quant. Spectrosc. Radiat. Transfer* **74** 539
[6] Olchawa W 2002 *J. Quant. Spectrosc. Radiat. Transfer* **74** 417
[7] Gigosos M A, Gonzalez M A and Cardenoso V 2003 *J. Spectrochim. Acta* B **58** 1489
[8] Olchawa W, Olchawa R and Grabowski B 2004 *Eur. Phys. J.* D **28** 119
[9] Touma J, Oks E, Alexiou S and Derevianko A 2000 *J. Quant. Spectrosc. Radiat. Transfer* **65** 543
[10] Oks E 2000 *J. Quant. Spectrosc. Radiat. Transfer* **65** 405
[11] Oks E 2002 *J. Phys. B: At. Mol. Opt. Phys.* **35** 2251
[12] Escarguel A, Oks E, Richou J and Volodko D 2000 *Phys. Rev.* E **62** 2667
[13] Flih S A, Oks E and Vitel Y 2003 *J. Phys. B: At. Mol. Opt. Phys.* **36** 283
[14] Escarguel , Ferhat B, Lesage A and Richou J 2000 *J. Quant. Spectrosc. Radiat. Transfer* **64** 353
[15] Flih S A and Vitel V 2001 *Proc. 15th Int. Conf. on Spectral Line Shapes* ed J Seidel vol 11 p 30
[16] Bock F, Stange M and Helbig V 2001 *Proc. 15th Int. Conf. on Spectral Line Shapes (AIP Conf. Proc.* No. 559*)* ed J Seidel (New York: American Institute of Physics) p 58
[17] Büscher S, Wrubel Th, Ferri S and Kunze H-J 2002 *J. Phys. B: At. Mol. Opt. Phys.* **35** 2889
[18] Böddeker St, Günter S, Könies A, Hitzschke L and Kunze H-J 1993 *Phys. Rev.* E **47** 2785
[19] Ispolatov Y and Oks E 1994 *J. Quant. Spectrosc. Radiat. Transfer* **51** 129
[20] Oks E 1997 *J. Quant. Spectrosc. Radiat. Transfer* **58** 821
[21] Kepple P and Griem H R 1968 *Phys. Rev.* **173** 317
[22] Griem H R 1974 *Spectral Line Broadening by Plasmas* (New York: Academic)
[23] Griem H R 1997 *Principles of Plasma Spectroscopy* (Cambridge: Cambridge University Press)
[24] Griem H R 1983 *Phys. Rev.* A **28** 1596
[25] Griem H R 1988 *Phys. Rev.* A **38** 2943
[26] Griem H R and Halenka J 2004 *Proc. 17th Int. Conf. on Spectral Line Shapes* ed E Dalimier (Paris: Frontier) p 442
[27] Griem H R 2001 *Phys. Rev.* E **64** 058401
[28] Griem H R 2003 *J. Phys. B: At. Mol. Opt. Phys.* **36** 1279
[29] Halenka J 2004 *Phys. Rev.* E **69** 028401
[30] Alexiou S 2002 *Spectral Line Shapes (AIP Conf. Proc.* vol 645*)* vol 12 (New York: American Institute of Physics) p 302
Alexiou S 2003 *J. Quant. Spectrosc. Radiat. Transfer* **81** 13

[31] Stamm R and Voslamber D 1979 *J. Quant. Spectrosc. Radiat. Transfer* **22** 599
[32] Seidel J and Stamm R 1982 *J. Quant. Spectrosc. Radiat. Transfer* **27** 499
[33] Gigosos M A, Cardeñoso V and Torres F 1986 *J. Phys. B: At. Mol. Phys.* **19** 3027
[34] Hegerfeldt G C and Kesting V 1988 *Phys. Rev.* A **37** 1488
[35] Kesting V 1992 *PhD Thesis* Georg-August-Universität, Göttingen
[36] Alexiou S 1996 *Phys. Rev. Lett* **76** 1836
[37] Halenka J and Olchawa W 1996 *J. Quant. Spectrosc. Radiat. Transfer* **56** 17
[38] Sholin G V, Demura A V and Lisitsa V S 1973 *Sov. Phys.—JETP* **37** 1057
[39] Mozer B and Baranger M 1960 *Phys. Rev.* **118** 626
[40] Pfenning H and Treffz E 1966 *Z. Naturforsch.* a **21** 697
[41] Hooper C F Jr 1968 *Phys. Rev.* **165** 215
[42] Alexiou S and Poquerusse A 2004 *Proc. 17th Int. Conf. on Spectral Line Shapes* ed E Dalimier (Paris: Frontier) p 457
[43] Hooper C F Jr 1966 *Phys. Rev.* **149** 77
[44] Wujec T, Olchawa W, Halenka J and Musielok J 2002 *Phys. Rev.* E **66** 066403
[45] Vitel Y, El Bezzari M, D'Yachkov L G and Kurilenkov Yu 1998 *Phys. Rev.* E **58** 7855
[46] Striganov A R and Sventitskii N S 1968 *Tables of Spectral Lines of Neutral and Ionized Atoms* (New York: Plenum)
de Broin T L, Humphreys C J and Meggers W F 1933 *Bur. Std. J. Res.* **11** 409
[47] Ralchenko Yu V 2003 Private communication
[48] Konjević N, Lesage A, Fuhr J R and Wiese W L 2002 *J. Phys. Chem. Ref. Data* **31** 819
[49] Inglis D R and Teller E 1939 *Astrophys. J.* **90** 439
[50] D'yachkov L G, Kurilenkov Y K and Vitel Y 1998 *J. Quant. Spectrosc. Radiat. Transfer* **59** 33
[51] Vitel Y 1987 *J. Phys. B: At. Mol. Opt. Phys.* **20** 2327
[52] Salohov M H, Sarandaev E W, Latipov R Z and Fishman I S 1986 *Opt. Spectrosc.* **60** 431
Salohov M H, Sarandaev E W, Latipov R Z and Fishman I S 1986 *Opt. Spectrosc.* **60** 264 (Engl. Transl.)
[53] Griem H R 1964 *Plasma Spectroscopy* (New York: McGraw-Hill)
[54] Baebés A, Gigosos M A and GonzÍez 2001 *J. Quant. Spectrosc. Radiat. Transfer* **68** 679
[55] Lisitsa V S 1977 *Usp. Fiz. Nauk* **122** 449
Lisitsa V S 1977 *Sov. Phys.—Usp.* **20** 603
[56] Sobelman I I, Vainshtein L A and Yukov E A 1981 *Excitation of Atoms and Broadening of Spectral Lines* (Berlin: Springer)
[57] Stehle C 1999 *Ftp:/cdsarc.u-strasbg.fr/cats/VI/92A*
[58] Gigosos M A and Cardeñoso V 1996 *J. Phys. B: At. Mol. Opt. Phys.* **29** 4795
[59] Griem H R, Baranger M, Kolb A C and Oertel G 1962 *Phys. Rev.* **125** 177
[60] Oks E 2003 *J. Phys. B: At. Mol. Opt. Phys.* **36** 1459
[61] Oks E 1994 *Phys. Rev. Lett.* **73** 2059
[62] Oks E 1994 *J. Quant. Spectrosc. Radiat. Transfer* **54** 307
[63] Parigger Ch G, Plemmons D H and Oks E 2003 *Appl. Opt.* **42** 5992
[64] Günter S, Hitzschke L and Röpke G 1991 *Phys. Rev.* A **44** 6834
[65] Alexiou S and Leboucher-Dalimer E 1999 *Phys. Rev.* E **60** 3436
[66] Wujec T, Jazgara A, Halenka J and Musielok J 2003 *Eur. Phys. J.* D **23** 405
[67] Lochte-Holtgreven W (ed) 1968 *Plasma Diagnostics* (Amsterdam: North-Holand)
[68] Halenka J 1990 *Z. Phys. D: At. Mol. Cluster* **16** 1
[69] Nick K-P, Richter J and Helbig V 1984 *J. Quant. Spectrosc. Radiat. Transfer* **32** 1